

$2\alpha + t$ cluster feature of $3/2^-$ state in ^{11}B

Yoshiko Kanada-En'yo

Department of Physics, Kyoto University, Kyoto 606-8502, Japan

Tadahiro Suhara

Matsue College of Technology, Matsue 690-8518, Japan

We reanalyze $2\alpha + t$ cluster features of $3/2^-$ states in ^{11}B by investigating the t cluster distribution around a 2α core in ^{11}B , calculated with the method of antisymmetrized molecular dynamics (AMD). In the $3/2^-$ state, a t cluster is distributed in a wide region around 2α , indicating that the t cluster moves rather freely in angular as well as radial motion. From the weak angular correlation and radial extent of the t cluster distribution, we propose an interpretation of a $2\alpha + t$ cluster gas for the $3/2^-$ state. In this study, we compare the $2\alpha + t$ cluster feature in $^{11}\text{B}(3/2^-)$ with the 3α cluster feature in $^{12}\text{C}(0_2^+)$, and discuss their similarities and differences.

I. INTRODUCTION

Many cluster structures have been found in light nuclei, such as ^7Li with an $\alpha + t$ cluster and ^8Be with a 2α cluster. In the excited states of ^{12}C , various 3α cluster structures have been discovered (for example, Refs. [1, 2] and references therein). In the early stages, the possibility of a linear 3α chain structure was proposed for $^{12}\text{C}(0_2^+)$ by Morinaga *et al.* [3, 4]. However, the linear chain structure of $^{12}\text{C}(0_2^+)$ has been excluded by the α decay width of this state [5]. Later theoretical studies with 3α cluster models have revealed that $^{12}\text{C}(0_2^+)$ is a weakly bound 3α state with neither geometric structures of the linear chain nor triangle structures [6–14]. Further extended models that do not rely on assumptions of the existence of clusters have also obtained similar results of the cluster feature in $^{12}\text{C}(0_2^+)$ [15–18].

In 2001, Tohsaki *et al.* proposed a new interpretation of $^{12}\text{C}(0_2^+)$ [19], i.e., the “ α cluster gas” in which α clusters are weakly interacting like a gas [20–24]. In such a dilute cluster system, α particles behave as bosonic particles; therefore, this state has been discussed in relation to the α condensation predicted in dilute infinite matter [25]. The cluster gas phenomenon has been attracting great interest because it is a new concept of the cluster state and is different from the traditional concept of geometric cluster structures, in which clusters are localized and have a specific spatial configuration. Indeed, in this decade, theoretical and experimental studies of nuclei, such as ^8He , ^{10}Be , ^{11}B , and ^{16}O , have included intensive searching for cluster gas states [26–38].

For ^{11}B , a developed $2\alpha + t$ cluster structure in the $3/2^-$ state was predicted by a $2\alpha + t$ cluster model [39] and the method of antisymmetrized molecular dynamics (AMD) [27, 35]. The $3/2^-$ state at 8.56 MeV is assigned to this $2\alpha + t$ state because the experimentally measured $M1$ and monopole transition strengths [26, 40] and the GT transition strength of the mirror state [41] are reproduced by the calculation. Studies have found similarity between $^{11}\text{B}(3/2^-)$ and $^{12}\text{C}(0_2^+)$ in remarkable monopole transitions and also predicted a nongeometric cluster feature of the $2\alpha + t$ structure in $^{11}\text{B}(3/2^-)$ similar to that of the 3α cluster structure in $^{12}\text{C}(0_2^+)$ [26, 27, 35]. From the analogies to $^{12}\text{C}(0_2^+)$, $^{11}\text{B}(3/2^-)$ was interpreted as a $2\alpha + t$ cluster gas.

However, the cluster gas in a $2\alpha + t$ system has not been fully understood. The following problems remain to be clarified. First, the parity of the $2\alpha + t$ state is negative and conflicts with the original idea of cluster gas, in which α clusters occupy an S orbit [33] and form a positive parity state. How can we extend the α cluster gas picture to the $3/2^-$ state containing a t cluster with negative parity? Second, it is not obvious whether the $2\alpha + t$ cluster state shows a nongeometric feature because a state with three clusters is more bound in the $2\alpha + t$ system than in the 3α system, resulting in a smaller size of $^{11}\text{B}(3/2^-)$ than that of $^{12}\text{C}(0_2^+)$ because of the deeper effective potential between t and α clusters than that between two α clusters.

In this study, we reanalyze the ^{11}B and ^{12}C wave functions obtained by AMD calculations in previous studies [16, 27] and investigate the motion of a t cluster around 2α . We pay particular attention to the angular motion of the t cluster with respect to the 2α orientation to judge whether the $2\alpha + t$ structures in ^{11}B have a geometric feature with an angular correlation or a nongeometric structure with weak angular correlation similar to the 3α gas state of $^{12}\text{C}(0_2^+)$. We also discuss the analogy and differences between $2\alpha + t$ structures in ^{11}B and 3α structures in ^{12}C . By considering the body-fixed plane of three clusters, we can connect the P -wave motion of the t cluster around 2α to the S -wave motion of the α cluster around 2α , and then extend the picture of the 3α cluster gas to the $2\alpha + t$ system.

The paper is organized as follows. We describe the AMD and cluster models in Section II. Section III discusses cluster structures of $3/2^-$ states of ^{11}B , in comparison with those of 0^+ states of ^{12}C . The paper concludes with a summary in section IV.

II. FORMULATION

In Refs. [16, 27], $3/2^-$ states of ^{11}B and 0^+ states of ^{12}C have been calculated with the AMD model. In the present study, we reanalyzed the AMD wave functions of ^{11}B and ^{12}C obtained in previous studies by using the $2\alpha + t$ and 3α cluster model wave functions written by the Brink-Bloch (BB) model [42]. In this section, we briefly explain the AMD model adopted in previous studies and describe the BB cluster wave function used in the present analysis.

A. AMD model

The AMD model is a useful approach to describe the formation and breaking of clusters as well as shell-model states having non-cluster structures [43, 44]. The applicability of the AMD method to light nuclei has been proven [45–47]. In the previous studies of ^{11}B and ^{12}C , the variation after spin-parity projection (VAP) in the AMD framework was applied [16, 27]. For the detailed formulation of the AMD+VAP, please refer to the previously mentioned references.

A Slater determinant of Gaussian wave packets gives an AMD wave function of an A -nucleon system:

$$\Phi_{\text{AMD}}(\mathbf{Z}) = \frac{1}{\sqrt{A!}} \mathcal{A}\{\varphi_1, \varphi_2, \dots, \varphi_A\}, \quad (1)$$

$$\varphi_i = \phi_{\mathbf{X}_i} \sigma_i \tau_i, \quad (2)$$

$$\phi_{\mathbf{X}_i}(\mathbf{r}_j) = \left(\frac{2\nu}{\pi}\right)^{4/3} \exp\left\{-\nu\left(\mathbf{r}_j - \frac{\mathbf{X}_i}{\sqrt{\nu}}\right)^2\right\}, \quad (3)$$

$$\sigma_i = \left(\frac{1}{2} + \xi_i\right)\sigma_{\uparrow} + \left(\frac{1}{2} - \xi_i\right)\sigma_{\downarrow}, \quad (4)$$

where $\phi_{\mathbf{X}_i}$ and σ_i are spatial and spin functions of the i th single-particle wave function, respectively, and τ_i is the isospin function fixed to be up (proton) or down (neutron). Accordingly, an AMD wave function is expressed by a set of variational parameters, $\mathbf{Z} \equiv \{\mathbf{X}_1, \mathbf{X}_2, \dots, \mathbf{X}_A, \xi_1, \xi_2, \dots, \xi_A\}$. The width parameter ν is chosen to be a common value for all nucleons and it is taken to be $\nu = 0.19 \text{ fm}^{-2}$ for ^{11}B and ^{12}C .

In the AMD+VAP method, we perform energy variation after spin-parity projections in the AMD model space to obtain the wave function for the lowest J^π state. Namely, the parameters \mathbf{X}_i and ξ_i ($i = 1, \dots, A$) of the AMD wave function are varied to minimize the energy expectation value, $\langle \Phi | H | \Phi \rangle / \langle \Phi | \Phi \rangle$, with respect to the spin-parity eigenwave function projected from an AMD wave function, $\Phi = P_{MK}^{J^\pi} \Phi_{\text{AMD}}(\mathbf{Z})$. For excited J_k^π states, the variation is performed for the energy expectation value of the component of the projected AMD wave function $P_{MK}^{J^\pi} \Phi_{\text{AMD}}(\mathbf{Z})$, orthogonal to the lower J_i^π ($i = 1, \dots, k-1$) states.

In each nucleus, all AMD wave functions obtained for various J^π states are superposed to obtain final wave functions $\Psi_{\text{AMD+VAP}}(J_k^\pi)$ for J_k^π states by solving the Hill-Wheeler equation. To describe ^{11}B and ^{12}C , approximately, twenty independent AMD wave functions are adopted for basis wave functions in the superposition [16, 27]. Because the number of basis AMD wave functions is finite, continuum states cannot be treated properly in the present AMD+VAP method. The method is a bound state approximation in which resonance states are obtained as bound states.

In the AMD model space, we treat all single-nucleon wave functions as independent Gaussian wave packets, and therefore, cluster formation and breaking are described by spatial configurations of Gaussian centers, \mathbf{X}_i . If we choose a specific set of parameters $\{\mathbf{Z}\}$, the AMD wave function can be equivalent to a BB cluster wave function.

Note that the cluster-breaking component affects not only the ground state but also the excited cluster states of ^{12}C , as shown in Refs. [18, 48]. We should stress that the AMD model can describe various cluster structures while incorporating cluster-breaking effects.

B. Cluster model

To analyze t -cluster motion in the ^{11}B wave functions obtained by the AMD+VAP model, we measure the position of the t cluster around the 2α core by using the BB wave function, which expresses a three-center cluster wave function with a specific spatial configuration of cluster positions.

The BB wave function for a $2\alpha + t$ cluster structure of ^{11}B is described as

$$|\Phi_{\text{BB}}(\mathbf{R}_1, \mathbf{R}_2, \mathbf{R}_3)\rangle = \frac{1}{\sqrt{A!}} \mathcal{A}\{\psi_\alpha(\mathbf{R}_1)\psi_\alpha(\mathbf{R}_2)\psi_t(\mathbf{R}_3)\}. \quad (5)$$

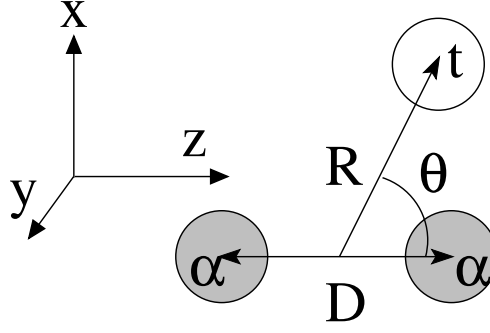


FIG. 1: Schematic figure of $2\alpha + t$ cluster structure.

Here $\psi_\alpha(\mathbf{R}_i)$ and $\psi_t(\mathbf{R}_i)$ are α - and t -cluster wave functions described by the harmonic oscillator $(0s)^4$ and $(0s)^3$ shell-model wave functions with the shifted center position \mathbf{R}_i , respectively. The width parameter of the harmonic oscillator is $\nu = 0.19 \text{ fm}^{-2}$, same as the AMD wave functions for ^{11}B and ^{12}C in the previous studies.

When clusters are far from each other and the antisymmetrization effect between clusters is negligible, \mathbf{R}_i indicates cluster center positions around which the α and t clusters are localized. In other words, the parameters \mathbf{R}_i ($i = 1, 2, 3$) specify the spatial configuration of cluster positions. Note that if \mathbf{R}_i are close to each other, the antisymmetrization effect is strong and \mathbf{R}_i does not necessarily have a physical meaning of the cluster position. For instance, in the small distance limit between cluster centers \mathbf{R}_i , the BB wave function no longer describes localized clusters but rather it describes a shell-model wave function.

We consider a configuration of three clusters, 2α and t , on the z - x plane at $y = 0$ with $(4\mathbf{R}_1 + 4\mathbf{R}_2 + 3\mathbf{R}_3)/11 = 0$. Two α clusters are set at the distance D with the orientation parallel to the z -axis as $\mathbf{R}_1 - \mathbf{R}_2 = (0, 0, D)$, and the t cluster is located at the distance R from the center of the 2α (see Fig. 1). We define the t -cluster position \mathbf{R} relative to the 2α center as

$$\mathbf{R} \equiv \mathbf{R}_3 - \frac{\mathbf{R}_1 + \mathbf{R}_2}{2} = (R \sin \theta, 0, R \cos \theta), \quad (6)$$

where the t -cluster direction is chosen at an angle θ from the z -axis (the 2α orientation).

To measure t cluster probability at a certain position, we calculate the overlap of the wave function, $\Psi_{\text{AMD+VAP}}(3/2_k^-)$, for $^{11}\text{B}(3/2_k^-)$ with the J^π -projected BB wave function

$$U(D, \mathbf{R}) = \langle P_{MK}^{J^\pi} \Phi_{\text{BB}}(\mathbf{R}_1, \mathbf{R}_2, \mathbf{R}_3) | \Psi_{\text{AMD+VAP}}(J_k^\pi) \rangle, \quad (7)$$

for $J^\pi = 3/2^-$. In the present study, the t intrinsic spin is set to the $+z$ direction and $K = +3/2$ is chosen so as to fix the z -component of the t orbital angular momentum to be $L_z^{(t)} = +1$.

If a t cluster is located far from 2α and the antisymmetrization effect between t and 2α is negligible, the relative wave function between the t cluster and 2α in the BB wave function is given by a Gaussian $\exp[-\gamma(\mathbf{r} - \mathbf{R})^2]$ with $\gamma = \sqrt{24/11}\nu$, i.e., the t cluster is well localized around \mathbf{R} . Therefore, the BB wave function can be regarded as the 'test function' for the t cluster, located at \mathbf{R} from the 2α core with the α - α distance D . The overlap of the test function with $\Psi_{\text{AMD+VAP}}(3/2_k^-)$ is roughly regarded as the t wave function on the z - x plane at $y = 0$, and its square stands for the t -cluster probability at \mathbf{R} around the 2α core.

In the present analysis, the normalization of Φ_{BB} is determined by the normalization of the constituent cluster wave functions $\psi_\alpha(\mathbf{R}_i)$ and $\psi_t(\mathbf{R}_i)$ before the antisymmetrization and projections. Namely, norms of $\psi_\alpha(\mathbf{R}_i)$ and $\psi_t(\mathbf{R}_i)$ are chosen independently of \mathbf{R}_i and are kept to be constant. They are determined to make the norm of the BB wave function $\Phi_{\text{BB}}(\mathbf{R}_1, \mathbf{R}_2, \mathbf{R}_3)$ to be a unit at the limit where cluster positions are far from each other and the antisymmetrization effect vanishes.

As cluster positions become close to each other, the norm of the BB wave function becomes smaller because of the antisymmetrization effect, which means that the cluster wave function, i.e., the t -cluster probability, is suppressed by Pauli blocking effect between nucleons in different clusters.

For a 3α system, we analyze the motion of an α cluster around the 2α core in a similar way to the t cluster in the $2\alpha + t$ system. The BB wave function for a 3α system is given by replacing the t cluster in Eq. 5 with an α cluster having a position \mathbf{R}_3 of $(4\mathbf{R}_1 + 4\mathbf{R}_2 + 4\mathbf{R}_3)/12 = 0$. A configuration of three α clusters on the z - x plane at $y = 0$ is considered, and we define the distance parameter D for the 2α core and the position \mathbf{R} for the α cluster around

the 2α in the same way as the $2\alpha + t$ case. To measure the α cluster probability at a certain position around the 2α core, we calculate the overlap of the wave function $\Psi_{\text{AMD+VAP}}(0_k^+)$ for $^{12}\text{C}(0_k^+)$ with the 0^+ -projected BB wave function. The overlap is regarded as the α -cluster wave function on the z - x ($y = 0$) plane, and its square stands for the probability of an α cluster at \mathbf{R} moving around the 2α core.

III. RESULTS

A. AMD+VAP wave functions for $^{11}\text{B}(3/2^-)$ and $^{12}\text{C}(0^+)$

We analyzed the AMD+VAP wave functions $\Psi_{\text{AMD+VAP}}(J_k^\pi)$ for $3/2_1^-$, $3/2_2^-$, and $3/2_3^-$ states of ^{11}B , and 0_1^+ , 0_2^+ , and 0_3^+ states of ^{12}C , which were obtained in previous studies [16, 27].

The adopted effective nuclear interactions is the MV1 force (case 3) [49] of the central force, supplemented by the spin-orbit term of the G3RS force [50]. The interaction parameters used in Ref. [27] for ^{11}B are $m = 0.62$, $b = h = 0.25$, and $u_{\text{ls}} = 2800$ MeV, and those in Ref. [16] for ^{12}C are $m = 0.62$, $b = h = 0$, and $u_{\text{ls}} = 3000$ MeV. We slightly modified the parameter set for ^{11}B from those for ^{12}C to obtain a better reproduction of energy levels of ^{11}B , as described in Ref. [16].

The ^{11}B wave functions are given by the superposition of $J^\pi = 3/2^-$ eigenwave functions projected from 17 basis AMD wave functions obtained by the VAP calculations, whereas ^{12}C wave functions are described by $J^\pi = 0^+$ eigenwave functions projected from 23 basis AMD wave functions.

Figure 2 shows the energy levels for $3/2^-$ states of ^{11}B and 0^+ states of ^{12}C . Compared with the experimental data, the interaction used in the previous studies tends to overestimate the relative energies to the threshold energies. We can improve the overestimation by changing the Majorana parameter m of the MV1 force. To obtain deeper binding wave functions than the original $m = 0.62$ results, we also perform calculations of ^{11}B and ^{12}C with the modified value $m = 0.60$ in solving the Hill-Wheeler equation, using the same basis AMD wave functions as in the original studies. We call the original parametrization "m62" and the modified one "m60". Figure 2 also shows the energy levels obtained with the m60 interaction. Interaction modification improves the energy positions of excited states. Because of the deeper binding, sizes of excited states and the radial motion of the t -cluster are slightly shrunk in the m60 result, as shown later. However, the feature of the t -cluster motion around 2α in ^{11}B is qualitatively unchanged by the modification from m62 to m60; therefore, in the present study, we mainly discuss the original m62 result.

Table I shows the calculated root mean square (rms) radii of matter density and rms charge radii. The experimental charge radii for the ground states are also listed. $^{11}\text{B}(3/2_3^-)$, $^{12}\text{C}(0_2^+)$, and $^{12}\text{C}(0_3^+)$ have remarkably larger radii than the ground states because these states have developed cluster structures.

As discussed in Ref. [16], $^{12}\text{C}(0_2^+)$ has no geometric structure, but it is described by the superposition of various configurations of three α clusters. This is consistent with calculations of the 3α cluster model [8] and the fermionic molecular dynamics [18] and the cluster gas picture proposed by Tohsaki *et al.* [19]. In contrast to $^{12}\text{C}(0_2^+)$, for $^{12}\text{C}(0_3^+)$, the AMD calculation predicts a geometric cluster feature, having a large overlap with the 3α cluster wave function with a chain-like 3α configuration.

For $^{11}\text{B}(3/2_3^-)$, the AMD+VAP wave function shows a geometric feature quite similar to those of $^{12}\text{C}(0_2^+)$. This wave function is described by the superposition of various configurations of 2α and t clusters, which means that three clusters are weakly interacting like a gas. Another analogy of $^{11}\text{B}(3/2_3^-)$ to $^{12}\text{C}(0_2^+)$ is strong monopole transition from the ground state [26]. This transition means that $^{11}\text{B}(3/2_3^-)$ is understood by radial excitation, similarly to $^{12}\text{C}(0_2^+)$, rather than by angular excitation. Because of these analogies of $^{11}\text{B}(3/2_3^-)$ to $^{12}\text{C}(0_2^+)$, an interpretation of the $2\alpha + t$ cluster gas state for $^{11}\text{B}(3/2_3^-)$ was proposed in the previous studies.

B. $\alpha + \alpha$ and $\alpha + t$ cluster systems

Because α - t and α - α effective interactions may give essential contributions to three-body cluster dynamics of $2\alpha + t$ and 3α systems, we here describe properties of subsystems, $\alpha + t$ and 2α systems, obtained by the present nuclear interactions.

^7Li and ^8Be are described well by $\alpha + t$ and 2α cluster models and they are regarded as weakly (quasi) bound two-body cluster states. The ground states of ^7Li and ^8Be are the $3/2_1^-$ and 0_1^+ states, respectively. The experimental ^7Li energy measured from the $\alpha + t$ threshold is -2.47 MeV and the ^8Be energy from the 2α threshold is 0.093 MeV. These facts indicate that clusters are bound relatively deeper in the $\alpha + t$ system than in the 2α system.

We calculate $^7\text{Li}(3/2_1^-)$ and $^8\text{Be}(0_1^+)$ with the generator coordinate method (GCM) using $\alpha + t$ and 2α cluster wave functions given by the BB model. The width parameter $\nu = 0.19$ fm $^{-2}$, same as for ^{11}B and ^{12}C wave functions, is used for α and t clusters. The distance parameters $D_{\alpha-\alpha}$ and $D_{\alpha-t}$ for the generator coordinate is taken to be

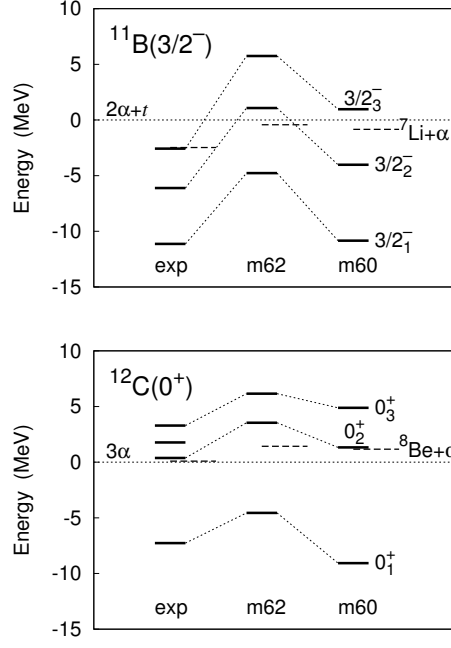


FIG. 2: Energies of $3/2^-$ states of ^{11}B measured from the $2\alpha + t$ threshold and those of 0^+ states of ^{12}C measured from the 3α threshold. $^7\text{Li}+\alpha$ and $^8\text{Be}+\alpha$ threshold energies are also shown. Theoretical values calculated using $m = 0.62$ and those for $m = 0.60$ are shown in comparison with the experimental energy levels.

TABLE I: The rms radii of matter density and rms charge radii calculated with the AMD+VAP using m62 and m60 interactions. The experimental charge radii are taken from Ref. [51]. The unit is fm.

	m62		m60		exp.
	matter	charge	matter	charge	charge
$^{11}\text{B}(3/2_1^-)$	2.5	2.6	2.5	2.6	2.406 (0.291)
$^{11}\text{B}(3/2_2^-)$	2.7	2.8	2.7	2.8	—
$^{11}\text{B}(3/2_3^-)$	3.0	3.1	3.0	3.0	—
$^{12}\text{C}(0_1^+)$	2.5	2.7	2.5	2.6	2.47 (0.022)
$^{12}\text{C}(0_2^+)$	3.3	3.4	3.0	3.2	—
$^{12}\text{C}(0_3^+)$	4.0	4.1	3.9	4.0	—

$D_{\alpha-\alpha(t)}=1, 2, \dots, 8$ fm, and resonance states are obtained as bound states within a bound state approximation in a finite volume. In the GCM calculation, the t - α binding obtained in ^7Li is deeper than the α - α binding in ^8Be . The energies of ^7Li and ^8Be measured from the α -decay threshold are -0.4 MeV and 1.4 MeV for the m62 case and -0.8 MeV and 1.2 MeV for the m60 case.

Figure 3 shows the $J^\pi = 3/2^-$ energy projected from a single BB model wave function for $\alpha + t$ and the 0^+ energy for 2α as functions of the intercluster distance $D_{\alpha-\alpha(t)}$. The figure also shows GCM amplitudes defined by the squared overlap of a J^π -projected BB wave function with the GCM wave functions. Here the J^π -projected BB wave function is normalized to have a unit norm. The energy curve shows the effective repulsion in a small distance region because of the Pauli blocking effect from the antisymmetrization. The effective repulsion is larger in the 2α system because of the stronger Pauli blocking and it pushes clusters outward, as seen in the GCM amplitudes. Also in the $\alpha + t$ system, clusters are developed spatially and distributed in an outer region because of the antisymmetrization effect in the inner region. Quantitatively, the $\alpha + t$ system is relatively deeper bound than the 2α system because of the weaker Pauli blocking as well as the attractive spin-orbit force.

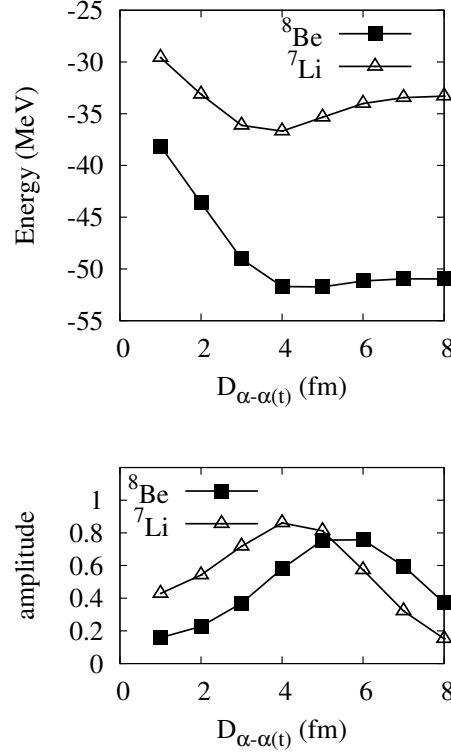


FIG. 3: (Upper) energy curve of the $\alpha + t$ system for ^7Li and that of the 2α system for ^8Be . The $J^\pi = 3/2^-$ and $J^\pi = 0^+$ projected energies are plotted as functions of the intercluster distance $D_{\alpha-\alpha(t)}$ of the BB cluster wave function. (Lower) GCM amplitudes for the $^7\text{Li}(3/2^-)$ state were obtained by the $\alpha + t$ cluster GCM calculation, and those for the $^8\text{Be}(0^+)$ state were obtained by the 2α cluster GCM calculation.

C. Cluster motion in ^{11}B and ^{12}C

In the previous study, we interpreted $^{11}\text{B}(3/2_3^-)$ as the $2\alpha + t$ cluster gas state because of the analogies of $^{11}\text{B}(3/2_3^-)$ to $^{12}\text{C}(0_2^+)$ in cluster features and the monopole transition. One characteristic of these cluster states is that the nongeometric feature of three cluster configuration is different from $^{12}\text{C}(0_3^+)$, which has a large overlap with the open triangle configuration. If the $2\alpha + t$ system has a nongeometric cluster structure, the t cluster around the 2α has weak angular correlation, and it shows wide distribution in angular motion. Therefore, the t distribution in the nongeometric cluster structure should be different from that in a geometric cluster structure, which concentrates at a certain angle, reflecting a specific configuration of cluster positions. In other words, the wide distribution of clusters in angular motion is an evidence of the nongeometric cluster structure, and it can be a probe for a cluster gas state, which is characterized by weak correlations in angular motion as well as in radial motion.

In the present analysis of cluster motion in $2\alpha + t$ and 3α systems, we consider the body-fixed frame in which the configuration of cluster positions is parametrized by \mathbf{R} for the t (α) position and D for the α - α distance of the 2α core, as explained before (see Fig. 1). In the body-fixed frame, the angular correlation is reflected by the angular distribution of the t (α) cluster around the 2α core.

1. Energy surface

Figure 4 shows the energy surface of the $2\alpha + t$ wave function on the (R_z, R_x) plane for the t position around a fixed 2α core with the α - α distance D and that of the 3α wave function for the α motion around a 2α . The energy

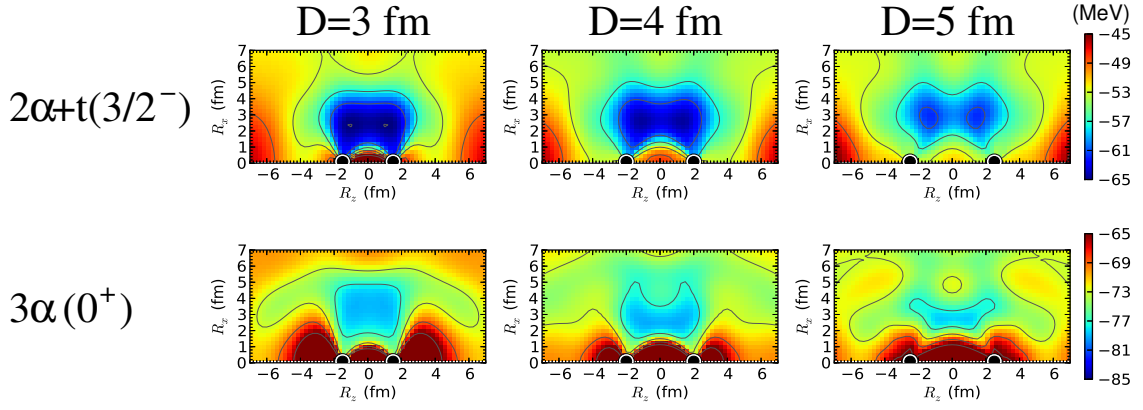


FIG. 4: (Color online) Energy of the $(J^\pi, K) = (3/2^-, +3/2)$ states projected from BB wave functions for the $2\alpha + t$ cluster and that of the 0^+ states for 3α cluster calculated with m62. This figure shows the energy surface on the (R_z, R_x) plane for a fixed 2α core with the 2α distance $D = 3, 4$, and 5 fm.

of the J^π -projected BB wave function given as

$$E_{2\alpha+t(\alpha)}(D, \mathbf{R}) \equiv \frac{\langle \Phi_{\text{BB}}(\mathbf{R}_1, \mathbf{R}_2, \mathbf{R}_3) P_{MK}^{J^\pi} | H | P_{MK}^{J^\pi} \Phi_{\text{BB}}(\mathbf{R}_1, \mathbf{R}_2, \mathbf{R}_3) \rangle}{\langle \Phi_{\text{BB}}(\mathbf{R}_1, \mathbf{R}_2, \mathbf{R}_3) P_{MK}^{J^\pi} | P_{MK}^{J^\pi} \Phi_{\text{BB}}(\mathbf{R}_1, \mathbf{R}_2, \mathbf{R}_3) \rangle} \quad (8)$$

for $(J^\pi, K) = (3/2^-, +3/2)$ states of $2\alpha + t$ and $J^\pi = 0^+$ states of 3α are calculated with the m62 interaction.

In the energy surface of $2\alpha + t$ for the t motion, the energy pocket at $R = 2$ – 3 fm for the 2α core with $D = 3$ fm corresponds to the ground state of ^{11}B . For the 2α core with $D = 4$ – 6 fm, the energy surface is soft in the $R = 4$ – 6 fm region against the angular motion as well as the radial motion of the t cluster. As shown later in this paper, $^{11}\text{B}(3/2_3^-)$ contains significant components of $2\alpha + t$ in this soft region. In the $\theta \sim 0$ and 180° region along the z -axis, the energy is relatively high, indicating that the linear configuration is unfavored. Also, in the energy surface of 3α for the α motion around the 2α core, the energy surface is soft for the 2α core with $D = 4$ – 6 fm in the angular and radial motions, except for the $\theta \sim 0$ and 180° regions. It is shown that the $\theta \sim 0$ and 180° configurations for the linear structure are unfavored also in the 3α system. From the softness of the energy surface, we expect that a t cluster or an α cluster can move around the 2α rather freely in the large R region, except for the $\theta \sim 0$ and 180° regions.

It should be noted that the $(J^\pi, K) = (3/2^-, +3/2)$ state of $2\alpha + t$ has a node at the z -axis and its component vanishes in the $\theta = 0$ and 180° configuration for the ideal linear structure. Although the energy of the $(J^\pi, K) = (3/2^-, +3/2)$ state can be calculated for the small R_x limit, the parameter R_x does not have a physical meaning of the t -cluster position in the $R_x < 1/\sqrt{2\gamma} \sim 1$ fm region.

2. Cluster motion in ^{11}B and ^{12}C

To investigate cluster motion in ^{11}B and ^{12}C , we calculate the overlap $U(D, \mathbf{R})$ between the BB wave function and the AMD+VAP wave function defined in Eq. 7. We focus on the \mathbf{R} dependence of $U(D, \mathbf{R})$ to see the t -cluster motion in ^{11}B and to compare it with that of the α -cluster motion in ^{12}C .

We show the R_x – R_z plot of the overlap $U(D, \mathbf{R})$ for each D for $^{11}\text{B}(3/2_1^-)$, $^{11}\text{B}(3/2_2^-)$, and $^{11}\text{B}(3/2_3^-)$ in Fig. 5 and that for $^{12}\text{C}(0_1^+)$, $^{12}\text{C}(0_2^+)$, and $^{12}\text{C}(0_3^+)$ in Fig. 6. The figures show the t -cluster motion and the α -cluster motion around a 2α core with the fixed α – α distance D . We also show the θ dependence of the $U(D, \mathbf{R})$ for $D = R = 3, 4$, and 5 fm cases in Fig. 7, which shows the angular distribution of the t cluster in ^{11}B and the α cluster in ^{12}C .

In $^{11}\text{B}(3/2_1^-)$, a remarkable peak at $(R_z, R_x) \sim (0, 3)$ fm for $D = 3$ fm indicates that clusters are confined in the inner region to form a compact triangle configuration of $2\alpha + t$. In contrast, $^{11}\text{B}(3/2_2^-)$ has a small overlap with the $K = +3/2$ component of $2\alpha + t$ cluster wave functions because this state is dominated by the $L = 2$ excitation of the 2α core and has a large overlap with the $K = -1/2$ component rather than with $K = +3/2$. This result is consistent with the discussion in previous study that $^{11}\text{B}(3/2_2^-)$ is the angular $\Delta L = 2$ excitation, having the weak monopole transition from the ground state, and it has a radius as small as the ground state; therefore, it is not a cluster gas state. In $^{11}\text{B}(3/2_3^-)$, the t cluster is not localized and its component is distributed in a wide area of R and θ in the

$R = 3\text{--}5$ fm region. The component in the inner region near the 2α core is suppressed because of the Pauli blocking between t and α clusters. Moreover, the component completely vanishes at the $R_x = 0$ line because of the trivial nodal structure at the z -axis of the t motion in the $L_z^{(t)} = +1$ orbit. Nevertheless, compared with the ground state, the $^{11}\text{B}(3/2_3^-)$ wave function has a wide distribution of the t cluster on the (R_x, R_z) plane, which means that the t cluster is not localized, but it moves rather freely, excluding the $\theta \sim 0$ and 180° regions. Furthermore, it contains significant $2\alpha + t$ components for a large α - α distance $D \geq 4$ fm of the 2α core. This information indicates that two α clusters in the 2α core are bound more weakly in $^{11}\text{B}(3/2_3^-)$ than in $^{11}\text{B}(3/2_1^-)$.

Features of α -cluster distributions in $^{12}\text{C}(0_1^+)$ and $^{12}\text{C}(0_2^+)$ are similar to the t distributions in $^{11}\text{B}(3/2_1^-)$ and $^{11}\text{B}(3/2_3^-)$, respectively. In $^{12}\text{C}(0_1^+)$, a significant peak of the overlap $U(D, \mathbf{R})$ exists at $(R_z, R_x) \sim (0, 3)$ fm for $D = 3$ fm, indicating the large overlap with a compact triangle configuration of 3α . In contrast to the ground state, the α cluster is not localized, but it is distributed in a wide area of R and θ in $^{12}\text{C}(0_2^+)$. The component in the region close to the z -axis, i.e., in the $\theta \sim 0$ and 180° regions, is suppressed because of the Pauli blocking effect from other α clusters in the core and because the linear 3α structure is energetically unfavored. As a result, the α distribution in the $R \leq 4$ fm region shows angular motion that is similar to that of the t distribution in $^{11}\text{B}(3/2_3^-)$. One characteristic of the α distribution in $^{12}\text{C}(0_2^+)$ that is different from the t distribution in $^{11}\text{B}(3/2_3^-)$ is the significant α distribution in the $R \geq 6$ fm region. In this region, far from the 2α core, the angular distribution of the α cluster in $^{12}\text{C}(0_2^+)$ becomes isotropic, showing S -wave feature differently than that of $^{11}\text{B}(3/2_3^-)$.

With $^{12}\text{C}(0_3^+)$, the α distribution is concentrated in the $|R_z| = 6\text{--}7$ fm and $R_x \leq 2$ fm region. The distribution indicates a remarkably developed 3α cluster structure, however, the angular motion of the α cluster in $^{12}\text{C}(0_3^+)$ is quite different from that in $^{12}\text{C}(0_2^+)$. $^{12}\text{C}(0_3^+)$ shows a strong angular correlation corresponding to the geometric configuration of the chain-like structure. This result contrasts with the weak angular correlation in $^{12}\text{C}(0_2^+)$, in which the α cluster is distributed in the wide θ region.

Note that the remarkable peak for the compact triangle configuration in the ground states of ^{11}B and ^{12}C originates in the antisymmetrization effect between clusters. In the region $R < 3$ fm, the cluster wave function is almost equivalent to the shell-model wave function. Because the quantum effect is significant in this region, \mathbf{R} has less meaning of the localization or position of clusters in the classical picture.

We also performed the same analysis for the ^{11}B and ^{12}C wave functions obtained with the m60 interaction, and found that the cluster motion is qualitatively the same as the m62 case, as shown in Fig. 8 for the m60 result, which corresponds to Fig. 7 for the m62 result.

3. Angular and radial motion in $^{11}\text{B}(3/2_3^-)$ and $^{12}\text{C}(0_2^+)$

To discuss the angular motion of the t cluster in $^{11}\text{B}(3/2_3^-)$ and compare it with the α cluster in $^{12}\text{C}(0_2^+)$ in more detail, we show the θ dependence of the overlap $U(D, \mathbf{R})$ for $R = 3\text{--}6$ fm in each D case in Fig. 9 for m62 and Fig. 10 for m60.

At $R = 3$ fm, the t distribution in $^{11}\text{B}(3/2_3^-)$ has a peak structure at $\theta = 90^\circ$, which means that the angular motion of the t cluster is restricted in the narrow θ region because of the Pauli blocking effect from α clusters. At $R = 4$ fm and 5 fm, the t cluster is distributed widely. In particular, at $R \geq 5$ fm, the t distribution becomes almost flat in the wide region of $30^\circ < \theta < 150^\circ$. Because of the node structure of the t motion in the $L_z^{(t)} = +1$ orbit, the t distribution vanishes at $\theta = 0$ and 180° in the $(J^\pi, K) = (3/2^-, +3/2)$ component of the $2\alpha + t$ system. As a result, the t cluster in $R \geq 5$ fm moves almost freely in the wide θ region, except for $\theta = 0$ and 180° regions for the trivial nodes.

In $^{12}\text{C}(0_2^+)$, the angular distribution of the α cluster at $R = 3$ fm has a peak at $\theta = 90^\circ$, similar to the t distribution in $^{11}\text{B}(3/2_3^-)$. As R increases, the angular distribution becomes wide. However, because the linear 3α configuration is energetically unfavored, the α distribution is somewhat suppressed in $\theta \sim 0$ and 180° regions at $R = 4, 5$ fm. At $R \geq 6$ fm, the angular distribution is almost flat in all θ regions, indicating that the α cluster moves freely in angular motion with no angular correlation.

Both $^{11}\text{B}(3/2_3^-)$ and $^{12}\text{C}(0_2^+)$ contain significant cluster distribution in the $R = 4\text{--}5$ fm region. In this region, the cluster around the 2α moves almost freely in angular motion with weak angular correlation. The present result indicates that these two states, $^{11}\text{B}(3/2_3^-)$ and $^{12}\text{C}(0_2^+)$, have a characteristic of a cluster gas in angular motion, if we tolerate the exclusion of the $\theta \sim 0$ and 180° regions.

Another characteristic of a cluster gas is a wide distribution of clusters in radial motion. The radial motion of the t cluster around the 2α at $\theta = 90^\circ$ in $^{11}\text{B}(3/2_1^-)$ and $^{11}\text{B}(3/2_3^-)$ and that of the α cluster in $^{12}\text{C}(0_1^+)$ and $^{12}\text{C}(0_2^+)$ are shown in Fig. 11. The t distribution in $^{11}\text{B}(3/2_1^-)$ is localized around $R = 3$ fm and rapidly damps as R increases. The suppression in the small R region comes from the antisymmetrization effect from the 2α . The α distribution in $^{12}\text{C}(0_1^+)$ has quite similar behavior to $^{11}\text{B}(3/2_1^-)$. In $^{11}\text{B}(3/2_3^-)$ and $^{12}\text{C}(0_2^+)$, the t (α) cluster around the 2α is distributed in the outer region widely, compared to distribution in the ground states. The cluster distribution is suppressed in the small R region, in particular, in the compact 2α core case with a small D because of the orthogonality to the ground

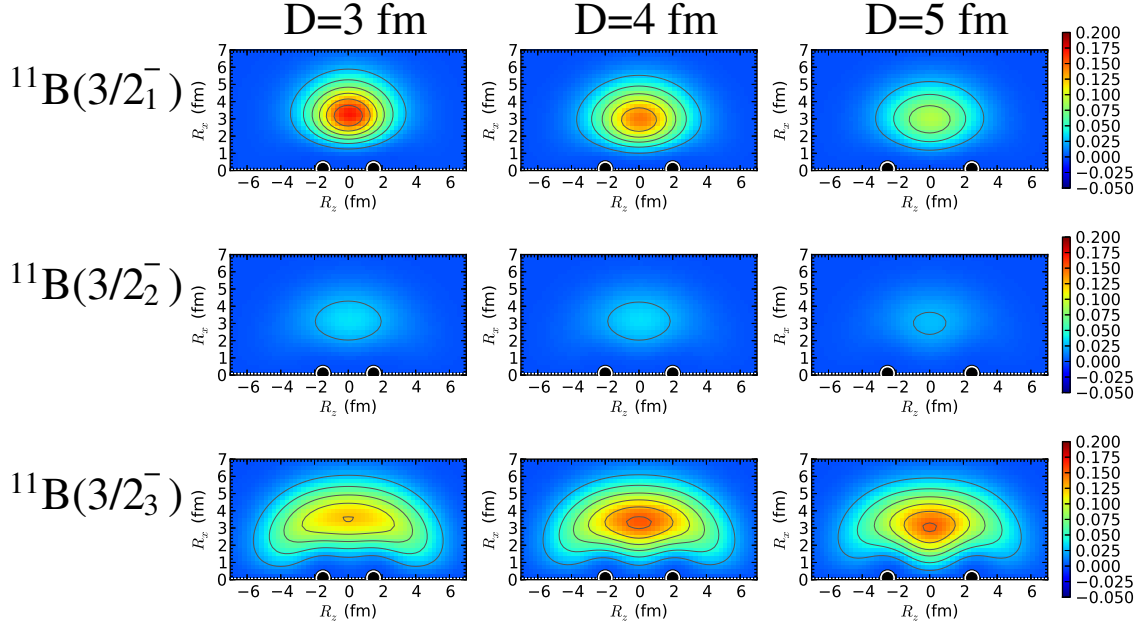


FIG. 5: (Color online) Overlap $U(D, \mathbf{R})$ of the BB wave function for $2\alpha + t$ cluster with the AMD+VAP wave functions for $^{11}\text{B}(3/2_1^-)$, $^{11}\text{B}(3/2_2^-)$, and $^{11}\text{B}(3/2_3^-)$ calculated with the m62 interaction. The overlap is plotted on the (R_z, R_x) plane for $D = 3, 4$, and 5 fm. The α positions $(R_z, R_x) = (\pm D/2, 0)$ in the 2α core are shown by black circles.

state as well as the antisymmetrization effect. The t distribution in $^{11}\text{B}(3/2_3^-)$ and the α distribution in $^{12}\text{C}(0_2^+)$ are outspread widely. In particular, the radial extent of the α distribution in $^{12}\text{C}(0_2^+)$ is remarkable, and that of the t distribution in $^{11}\text{B}(3/2_3^-)$ is relatively small. The relatively small extent in $^{11}\text{B}(3/2_3^-)$ originates in the deeper t - α binding than the α - α binding because of the weaker Pauli blocking effect between t and α clusters. As a result, the radial spreading of the t cluster in $^{11}\text{B}(3/2_3^-)$ is less remarkable than that of α cluster $^{12}\text{C}(0_2^+)$.

The D dependence of the overlap $U(D, \mathbf{R})$ shows the α - α radial motion in the 2α core. As seen in Fig. 11, in the ground states of ^{11}B and ^{12}C , the peak height of the overlap rapidly decrease as D increases, indicating that two α clusters are tightly bound to form a compact 2α core. In contrast, $^{11}\text{B}(3/2_3^-)$ and $^{12}\text{C}(0_2^+)$ contain a significant cluster component for $D = 3$ – 6 fm, indicating that the 2α core in these states is a weakly bound 2α cluster. The radial extent of the 2α in $^{11}\text{B}(3/2_3^-)$ is as large as that in $^{12}\text{C}(0_2^+)$. In other words, two α clusters in $^{11}\text{B}(3/2_3^-)$ behave as an α cluster gas.

D. Analogies of and differences in $2\alpha + t$ and 3α cluster gas states

As mentioned previously, $^{11}\text{B}(3/2_3^-)$ and $^{12}\text{C}(0_2^+)$ contain a significant cluster distribution in the $R = 4$ – 5 fm region. In this region, the cluster around the 2α core moves rather freely in the angular mode in a wide θ region, except for the $\theta \sim 0$ and 180° regions. For $^{11}\text{B}(3/2_3^-)$, the $L_z^{(t)} = +1$ motion of the t cluster in the $(J^\pi, K) = (3/2^-, +3/2)$ component of the $2\alpha + t$ wave function elementarily has the node structure at the z -axis. We know that the topological structure of the P wave motion for the t cluster is different from that of the S wave motion for the α cluster, experiencing neither node nor phase change in angular motion. However, when we consider the 2D cluster motion in the intrinsic frame, the angular motion of the t cluster in the $2\alpha + t$ system can be associated with that of the α cluster in the 3α system, as follows.

The α cluster distribution around the 2α core tends to be suppressed at $\theta = 0$ and 180° because of the Pauli blocking effect from the 2α core on the z -axis and also because of the energy loss in the linear 3α configuration. Let us consider the angular motion in the extreme case of $D = 2R$. In the angular distribution of the α cluster moving around the 2α , the probability completely vanishes at $\theta = 0$ and 180° because of the Pauli exclusion principle between nucleons in different α clusters. This situation is analogous to the angular distribution of the t cluster in the P wave with $L_z^{(t)} = +1$, in which the t probability vanishes at $\theta = 0$ and 180° . It should be noted that the sign of the α wave

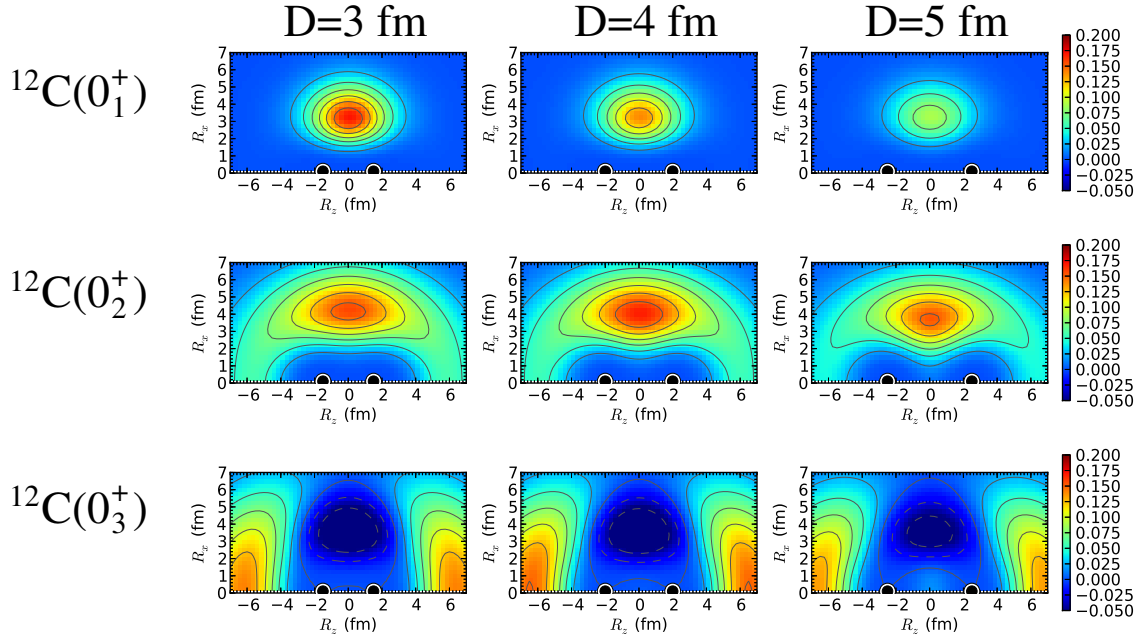


FIG. 6: (Color online) Overlap $U(D, \mathbf{R})$ of the BB wave function for a 3α cluster with the AMD+VAP wave functions for $^{12}\text{C}(0_1^+)$, $^{12}\text{C}(0_2^+)$, and $^{12}\text{C}(0_3^+)$, calculated with the m62 interaction. The overlap is plotted on the (R_z, R_x) plane for $D = 3, 4$, and 5 fm. The α positions $(R_z, R_x) = (\pm D/2, 0)$ in the 2α core are shown by black circles.

function is the same in $0 < \theta < 180^\circ$ and $180^\circ < \theta < 360^\circ$, but the sign of the t wave function in $180^\circ < \theta < 360^\circ$ is opposite to that in $0 < \theta < 180^\circ$. The opposite sign for a t wave function is a consequence of the negative parity of the total $2\alpha + t$ system, which originally comes from the negative parity of the lowest allowed orbit for the t - α intercluster motion, because the t cluster consists of odd-numbered fermions. By taking the absolute value of the t -cluster angular wave function, having two nodes at $\theta = 0$ and 180° around the 2α in the $2\alpha + t$ system, we can obtain an angular distribution similar to the α distribution around the 2α in the 3α system, which means that the one-dimensional t motion in the angular mode around the fixed 2α core can be mapped on the α motion around 2α . In three-dimensional space, the phase of the t wave function of the $L_z^{(t)} = +1$ orbit changes by 2π in the rotation around the z -axis. Again by taking the absolute value of the t wave function, it may be possible to consider a mapping of the t -cluster motion onto the α -cluster motion, if the α probability is suppressed at $\theta = 0$ and 180° .

In the 3α system for $^{12}\text{C}(0_2^+)$, the α probability is somewhat suppressed at $\theta = 0$ and 180° in the $R \leq 5$ fm region. In this region, the angular motion of the t cluster in $^{11}\text{B}(3/2_3^-)$ has some association with the α -cluster motion in $^{12}\text{C}(0_2^+)$, as described previously. That is, the cluster motion in both cases is characterized by the wide angular distribution, except for the $\theta = 0$ and 180° regions. However, this t -cluster and α -cluster association in the angular motion around the 2α breaks down in the asymptotic region, far from the 2α core. The α cluster distribution is isotropic and goes to the ideal S -wave motion in the asymptotic region, where the blocking effect from the core vanishes; by comparison, the t cluster in a P wave always has the node structure in the angular mode, even in the asymptotic region. Nevertheless, the t cluster in $^{11}\text{B}(3/2_3^-)$ is distributed in a wide θ region around the 2α , indicating that the total system has a non-geometric cluster structure with weak angular correlation rather than a geometric structure. If we tolerate the exclusion of $\theta \sim 0$ and 180° regions and extend the concept of the cluster gas as a developed cluster structure with weak angular correlation, $^{11}\text{B}(3/2_3^-)$ can be interpreted as a kind of cluster gas of $2\alpha + t$.

Therefore we can state the following:

- $^{11}\text{B}(3/2_3^-)$ and $^{12}\text{C}(0_2^+)$ are $2\alpha + t$ and 3α cluster states with weak angular correlation, like a cluster gas.

In addition to the similarity of and difference in the angular correlation mentioned previously, the following similarities and differences exist in the $2\alpha + t$ cluster structure of $^{11}\text{B}(3/2_3^-)$ and the 3α cluster structure of $^{12}\text{C}(0_2^+)$.

- In the radial motion of the t cluster around the 2α , the t distribution is outspread widely in $^{11}\text{B}(3/2_3^-)$, compared with the ground state, and it is similar to the radial motion of the α cluster in $^{12}\text{C}(0_2^+)$. However, the radial

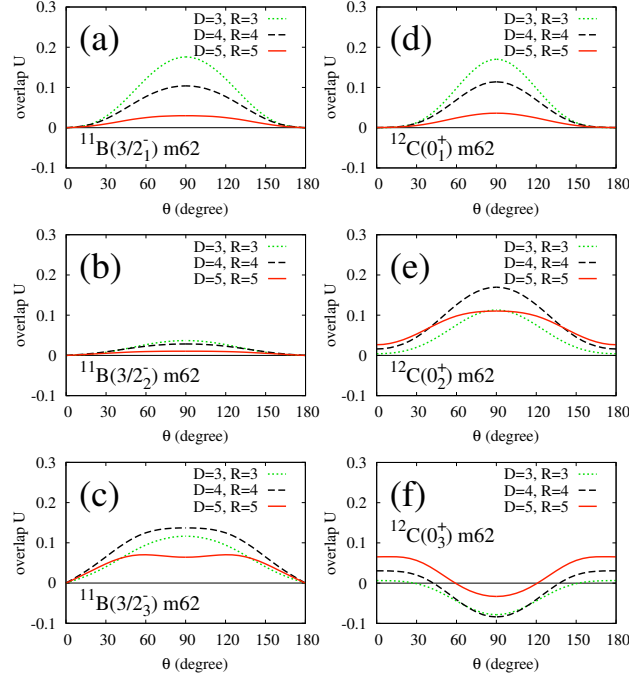


FIG. 7: (Color online) θ dependence of overlap $U(D, \mathbf{R})$ for ^{11}B and ^{12}C calculated with the m62 interaction in the $R = D$ case.

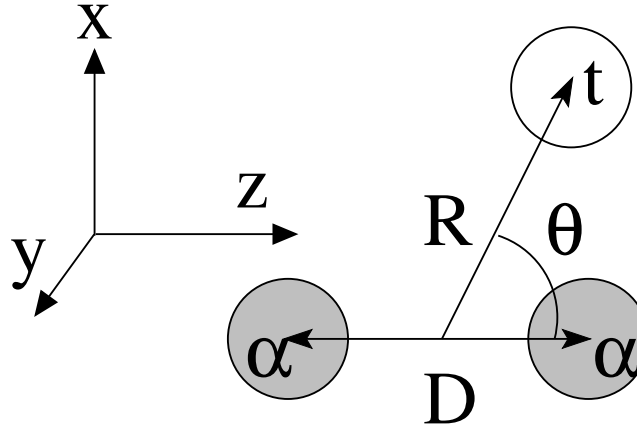


FIG. 8: (Color online) Same as Fig. 7; However, it is for the m60 result.

extent of the t distribution in $^{11}\text{B}(3/2_3^-)$ is relatively smaller than that of the α distribution in $^{12}\text{C}(0_2^+)$ because the t - α binding is deeper than the α - α binding, which occurs because of the weaker Pauli blocking between t and α clusters.

- The D dependence of the overlap $U(D, \mathbf{R})$ indicates that two α clusters in ^{11}B are bound as weakly as those in ^{12}C .

In conclusion, $^{11}\text{B}(3/2_3^-)$ is interpreted as a three-body cluster gas of $2\alpha + t$ in weak angular correlation and the radial extent of clusters. The cluster gas feature is more prominent in $^{12}\text{C}(0_2^+)$ than in $^{11}\text{B}(3/2_3^-)$.

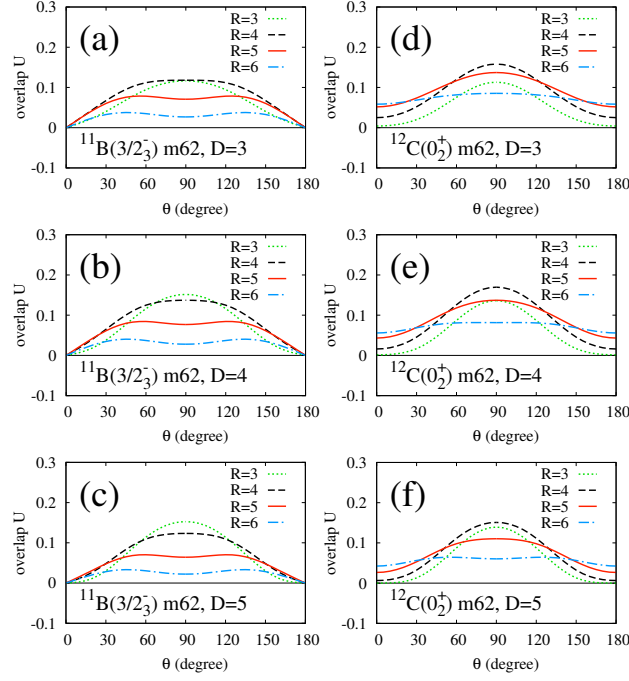


FIG. 9: (Color online) θ dependence of overlap $U(D, \mathbf{R})$ for $^{11}\text{B}(3/2_3^-)$ and $^{12}\text{C}(0_2^+)$ calculated with the m62 interaction.

IV. SUMMARY

In this study, we reanalyzed cluster features of $3/2^-$ states of ^{11}B and 0^+ states of ^{12}C , obtained with the AMD+VAP method in previous study. The $2\alpha + t$ cluster structures of ^{11}B were compared with the 3α cluster structures of ^{12}C in the analysis of cluster distribution. We were particularly attentive to the t -cluster motion around the 2α core in the $2\alpha + t$ system. We considered the 2D cluster motion in the intrinsic frame, and investigated the cluster distribution on the 2D plane. To discuss the angular motion and radial motion of the t cluster in ^{11}B and those of the α cluster in ^{12}C , we studied the dependencies of the cluster distribution on the distance R and the angle θ for the cluster position from the 2α . In particular, we discussed the θ dependence to clarify the angular motion of the t cluster around the 2α .

$^{11}\text{B}(3/2_3^-)$ and $^{12}\text{C}(0_2^+)$ contain significant t - and α -cluster distributions in the radial distance $R = 4\text{--}5$ fm region. In this region, the t -cluster motion in $^{11}\text{B}(3/2_3^-)$ is characterized by the wide angular distribution, except for the $\theta = 0$ and 180° regions. It is associated with the angular motion of the α cluster in $^{12}\text{C}(0_2^+)$, where the α distribution in the $\theta = 0$ and 180° regions is somewhat suppressed. By comparing the $2\alpha + t$ cluster structure in $^{11}\text{B}(3/2_3^-)$ and the 3α cluster structure in $^{12}\text{C}(0_2^+)$, the following similarities and differences are found.

- In angular motion, $^{11}\text{B}(3/2_3^-)$ and $^{12}\text{C}(0_2^+)$ are $2\alpha + t$ and 3α cluster states with weak angular correlation, like a cluster gas.
- In radial motion of the t cluster around the 2α , the t distribution is outspread widely in $^{11}\text{B}(3/2_3^-)$, compared with the ground state. However, the radial extent of the t distribution in $^{11}\text{B}(3/2^-)$ is less than that of the α distribution in $^{12}\text{C}(0_2^+)$ because the t - α binding is deeper than the α - α binding.
- The D dependence of the overlap $U(D, \mathbf{R})$ indicates that two α clusters in ^{11}B are bound weakly as those in ^{12}C .

In conclusion, $^{11}\text{B}(3/2_3^-)$ is interpreted as a three-body cluster gas of $2\alpha + t$ in sense of weak angular correlation and radial extent of the clusters. The cluster gas feature is more prominent in $^{12}\text{C}(0_2^+)$ than in $^{11}\text{B}(3/2_3^-)$.

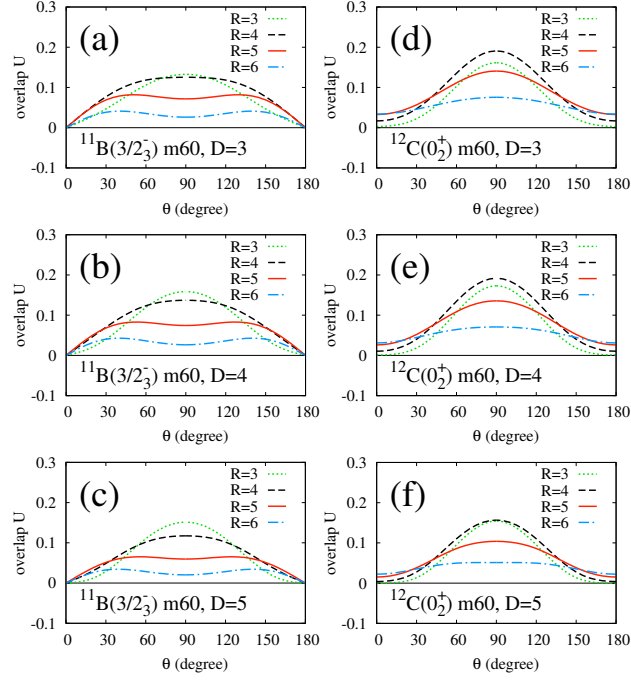


FIG. 10: (Color online) Same as Fig. 9 but for the m60 result.

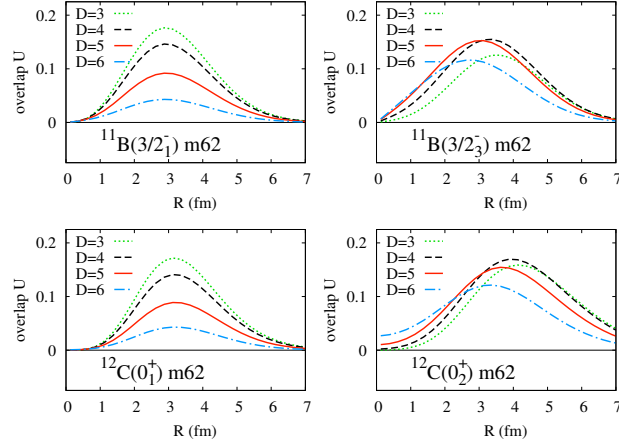


FIG. 11: (Color online) R dependence of $U(D, R)$ for $^{11}\text{B}(3/2_1^-)$, $^{11}\text{B}(3/2_3^-)$, $^{12}\text{C}(0_1^+)$, and $^{12}\text{C}(0_2^+)$ calculated with the m62 interaction.

Acknowledgments

The authors would like to thank Prof. Schuck for fruitful discussions. The computational calculations of this work were performed using the supercomputers at YITP. This work was supported by JSPS KAKENHI Grant Numbers

25887049 and 26400270.

-
- [1] Y. Fujiwara *et al.*, Prog. Theor. Phys. Suppl. **68**, 29 (1980).
 - [2] M. Freer and H. O. U. Fynbo, Prog. Part. Nucl. Phys. **78**, 1 (2014).
 - [3] H. Morinaga, Phys. Rev. **101**, 254 (1956).
 - [4] H. Morinaga, Phys. Lett. **21**, 78 (1966).
 - [5] Y. Suzuki, H. Horiuchi and K. Ikeda, Prog. Theor. Phys. **47**, 1517 (1972).
 - [6] Y. Fukushima and M. Kamimura, *Proc. Int. Conf. on Nuclear Structure, Tokyo, 1977, edited by T. Marumori* J. Phys. Soc. Jpn. **44**, 225 (1978).
 - [7] M. Kamimura, Nucl. Phys. **A351**, 456 (1981).
 - [8] E. Uegaki, S. Okabe, Y. Abe and H. Tanaka, Prog. Theor. Phys. **57**, 1262 (1977).
 - [9] E. Uegaki, Y. Abe, S. Okabe and H. Tanaka, Prog. Theor. Phys. **59**, 1031 (1978).
 - [10] E. Uegaki, Y. Abe, S. Okabe and H. Tanaka, Prog. Theor. Phys. **62**, 1621 (1979).
 - [11] P. Descouvemont and D. Baye, Phys. Rev. C **36**, 54 (1987).
 - [12] C. Kurokawa and K. Kato, Nucl. Phys. **A738**, 455 (2004).
 - [13] C. Kurokawa and K. Kato, Phys. Rev. C **71**, 021301(R) (2005).
 - [14] K. Arai, Phys. Rev. C **74**, 064311 (2006).
 - [15] Y. Kanada-En'yo, Phys. Rev. Lett. **81**, 5291 (1998).
 - [16] Y. Kanada-En'yo, Prog. Theor. Phys. **117**, 655 (2007) [Erratum-ibid. **121**, 895 (2009)].
 - [17] T. Neff and H. Feldmeier, Nucl. Phys. **A738**, 357 (2004).
 - [18] M. Chernykh, H. Feldmeier, T. Neff, P. von Neumann-Cosel and A. Richter, Phys. Rev. Lett. **98**, 032501 (2007).
 - [19] A. Tohsaki, H. Horiuchi, P. Schuck, and G. Röpke, Phys. Rev. Lett. **87**, 192501 (2001).
 - [20] Y. Funaki, H. Horiuchi, A. Tohsaki, P. Schuck and G. Ropke, Prog. Theor. Phys. **108**, 297 (2002).
 - [21] T. Yamada and P. Schuck, Phys. Rev. C **69**, 024309 (2004).
 - [22] Y. Funaki, A. Tohsaki, H. Horiuchi, P. Schuck and G. Ropke, Phys. Rev. C **67**, 051306 (2003).
 - [23] Y. Funaki, H. Horiuchi, W. von Oertzen, G. Ropke, P. Schuck, A. Tohsaki and T. Yamada, Phys. Rev. C **80**, 064326 (2009).
 - [24] T. Yamada, Y. Funaki, H. Horiuchi, G. Ropke, P. Schuck and A. Tohsaki, Lect. Notes Phys. **848**, 229 (2012).
 - [25] G. Röpke, A. Schnell, P. Schuck, and P. Nozieres, Phys. Rev. Lett. **80**, 3177 (1998).
 - [26] T. Kawabata, H. Akimune, H. Fujita, Y. Fujita, M. Fujiwara, K. Hara, K. Hatanaka and M. Itoh *et al.*, Phys. Lett. B **646**, 6 (2007).
 - [27] Y. Kanada-En'yo, Phys. Rev. C **75**, 024302 (2007).
 - [28] Y. Kanada-En'yo, Phys. Rev. C **76**, 044323 (2007).
 - [29] N. Itagaki, M. Kimura, C. Kurokawa, M. Ito and W. von Oertzen, Phys. Rev. C **75**, 037303 (2007).
 - [30] T. Wakasa, E. Ihara, K. Fujita, Y. Funaki, K. Hatanaka, H. Horiuchi, M. Itoh and J. Kamiya *et al.*, Phys. Lett. B **653**, 173 (2007).
 - [31] Y. Funaki, T. Yamada, H. Horiuchi, G. Ropke, P. Schuck and A. Tohsaki, Phys. Rev. Lett. **101**, 082502 (2008).
 - [32] Y. Funaki, T. Yamada, A. Tohsaki, H. Horiuchi, G. Ropke and P. Schuck, Phys. Rev. C **82**, 024312 (2010).
 - [33] T. Yamada and Y. Funaki, Phys. Rev. C **82**, 064315 (2010).
 - [34] S. Ohkubo, Y. Hirabayashi and Y. Hirabayashi, Phys. Lett. B **684**, 127 (2010).
 - [35] T. Suhara and Y. Kanada-En'yo, Phys. Rev. C **85**, 054320 (2012).
 - [36] T. Ichikawa, N. Itagaki, Y. Kanada-En'yo, T. Kokalova and W. von Oertzen, Phys. Rev. C **86**, 031303 (2012).
 - [37] F. Kobayashi and Y. Kanada-En'yo, Phys. Rev. C **86**, 064303 (2012).
 - [38] F. Kobayashi and Y. Kanada-En'yo, Phys. Rev. C **88**, no. 3, 034321 (2013).
 - [39] H. Nishioka, S. Saito and M. Yasuno, Prog. Theor. Phys. **62** 424 (1979).
 - [40] T. Kawabata, H. Akimune, H. Fujimura, H. Fujita, Y. Fujita, M. Fujiwara, K. Hara and K. Y. Hara *et al.*, Phys. Rev. C **70**, 034318 (2004).
 - [41] Y. Fujita *et al.*, Phys. Rev. C **70**, 011306(R) (2004).
 - [42] D.M. Brink, *Proceedings of the International School of Physics "Enrico Fermi"*, Varenna, 1965, Course 36, Ed. by C.Bloch (Academic Press, New York 1966)
 - [43] Y. Kanada-En'yo, H. Horiuchi and A. Ono, Phys. Rev. C **52**, 628 (1995).
 - [44] Y. Kanada-En'yo and H. Horiuchi, Phys. Rev. C **52**, 647 (1995).
 - [45] Y. Kanada-En'yo and H. Horiuchi, Prog. Theor. Phys. Suppl. **142**, 205 (2001).
 - [46] Y. Kanada-En'yo, M. Kimura and H. Horiuchi, Comptes rendus Physique Vol.4, 497 (2003).
 - [47] Y. Kanada-En'yo, M. Kimura and A. Ono, PTEP **2012** (2012) 01A202.
 - [48] in preparation.
 - [49] T. Ando, K. Ikeda and A. Tohsaki, Prog. Theor. Phys. **64**, 1608 (1980).
 - [50] N. Yamaguchi, T. Kasahara, S. Nagata and Y. Akaishi, Prog. Theor. Phys. **62**, 1018 (1979); R. Tamagaki, Prog. Theor. Phys. **39**, 91 (1968).
 - [51] I. Angeli, Atomic Data and Nuclear Data Tables **87**, 185 (2004).